Blood–brain and blood–cerebrospinal fluid passage of BRICHOS domains from two molecular chaperones in mice

Simone Tambaro, Lorena Galan-Acosta, Axel Leppert, Gefei Chen, Henrik Biverstål, Jenny Presto, Per Nilsson, and Jan Johansson[1]

From the Department of Neurobiology, Care Sciences and Society, Division of Neurogeriatrics, Karolinska Institutet, 141 83 Huddinge, Sweden

Edited by Ursula Jakob

Targeting toxicity associated with β-amyloid (Aβ) misfolding and aggregation is a promising therapeutic strategy for preventing or managing Alzheimer's disease. The BRICHOS domains from human prosurfactant protein C (proSP-C) and integral membrane protein 2B (Bri2) efficiently reduce neurotoxicity associated with Aβ42 fibril formation both *in vitro* and *in vivo*. In this study, we evaluated the serum half-lives and permeability into the brain and cerebrospinal fluid (CSF) of recombinant human (rh) proSP-C and Bri2 BRICHOS domains injected intravenously into WT mice. We found that rh proSP-C BRICHOS has a longer blood serum half-life compared with rh Bri2 BRICHOS and passed into the CSF but not into the brain parenchyma. As judged by Western blotting, immunohistochemistry, and ELISA, rh Bri2 BRICHOS passed into both the CSF and brain. Intracellular immunostaining for rh Bri2 BRICHOS was observed in the choroid plexus epithelium as well as in the cerebral cortex. Our results indicate that intravenously administered rh proSP-C and Bri2 BRICHOS domains have different pharmacokinetic properties and blood–brain/blood–CSF permeability in mice. The finding that rh Bri2 BRICHOS can reach the brain parenchyma after peripheral administration may be harnessed in the search for new therapeutic strategies for managing Alzheimer's disease.

Many neurodegenerative disorders such as Parkinson's disease, Huntington's disease, and Alzheimer's disease (AD)[2] are strongly linked with the accumulation of specific misfolded proteins (1). AD is the most common neurodegenerative disease, and it is characterized by the presence in the brain of extracellular plaques of β-amyloid (Aβ) peptide and by intracellular tangles of hyperphosphorylated tau proteins (2). The causes of AD are not clear, but the "amyloid cascade hypothesis" has been brought forward as one driving factor. The levels of Aβ start to increase 20 years before onset of the disease and lead to formation of β-sheet oligomers and fibrils that contribute to the onset of AD (3, 4). The Aβ peptide is derived from the Aβ precursor protein (AβPP), an integral membrane protein, by sequential proteolytic processing by β- and γ-secretases. The γ-secretase cleaves AβPP in the transmembrane region, resulting in Aβ peptides of varying length, most commonly 40 or 42 residues, of which the AD-associated Aβ42 is the more neurotoxic and aggregation-prone variant. Mutations in AβPP and in the enzymatic component of γ-secretase, presenilin 1, increase the levels of Aβ42 and cause early-onset familiar AD. Soluble oligomers of Aβ have been suggested as key components for causing synaptic and cognitive dysfunction because the correlation between synaptic loss and levels of soluble Aβ species is stronger than the correlation with plaque levels (5). To date, no curative therapies for AD exist; the current treatments only alleviate the symptoms of the disease and are effective merely in the early stages (6).

The BRICHOS domain consists of about 100 amino acid residues and has been found in more than 10 human transmembrane protein families, which are processed by proteolysis into fragments with different biological functions (7, 8). The different BRICHOS-containing proteins show overall low sequence conservation but have a conserved architecture (9) consisting of an N-terminal cytosolic part, a transmembrane part, a linker, the BRICHOS domain, and, in all cases except prosurfactant protein C (proSP-C), a C-terminal region that has a high predicted β-sheet propensity (8, 10). ProSP-C instead has a uniquely β-prone transmembrane region (11). Recombinant BRICHOS domains from the proteins associated with amyloid lung disease (proSP-C) and brain amyloid and dementia (integral membrane protein 2B (ITM2B or Bri2)) efficiently delay Aβ42 fibril formation *in vitro* (9, 12–15). The rh proSP-C BRICHOS domain specifically blocks the surface-catalyzed secondary nucleation step during Aβ42 fibril formation (16), whereas rh Bri2 BRICHOS inhibits both the secondary nucleation and Aβ42 fibril elongation steps (17, 18). In recent *in vivo* studies, overexpression of proSP-C or Bri2 BRICHOS delayed Aβ42 aggregation and improved the lifespan and locomotor function in a *Drosophila melanogaster* AD model (19, 20).
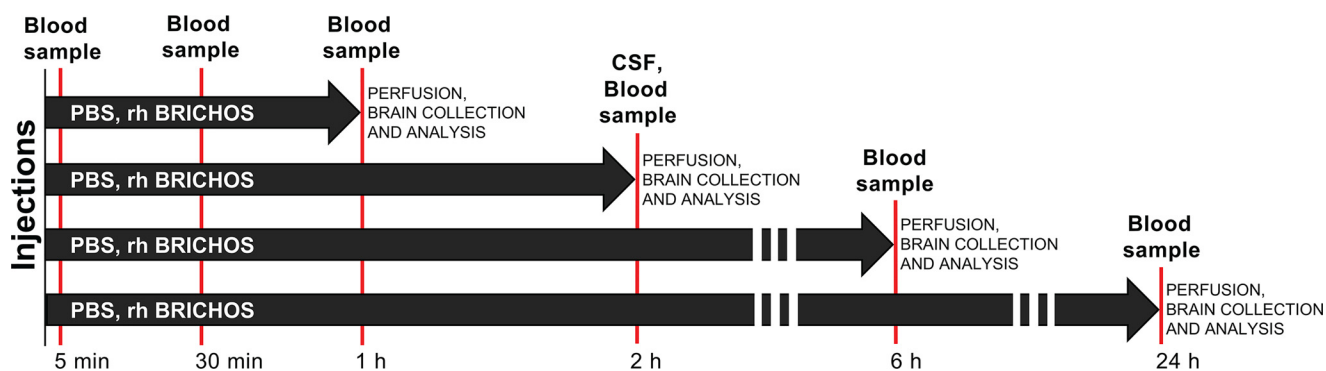
Although proSP-C is exclusively expressed in the alveolar epithelium (21, 22), Bri2 is ubiquitously expressed, and in the brain it is particularly abundant in CA1 pyramidal neurons (23, 24). Altered levels of Bri2 together with its processing enzymes

Figure 1. Overview of the study. Timeline of rh proSP-C and Bri2 BRICHOS injections and sampling of blood, CSF, and brain tissue for the different experiments.

and the homologue Bri3 (also called ITM2C) have been detected in the hippocampus of post-mortem AD cases (25, 26). Furthermore, the secreted Bri2 BRICHOS domain has been found to be associated with amyloid plaques (25).

Based on these findings, the BRICHOS domain has emerged as a new candidate among therapeutic strategies against AD. However, the neuroprotective function of the blood–brain barrier (BBB) together with the blood–cerebrospinal fluid barrier (BCSFB) represents a potential major obstacle for the delivery of BRICHOS into the central nervous system (CNS). The BBB consists of brain capillary endothelial cells joined together by tight junctions and surrounded by pericytes, astrocytes, and neuronal cells (27). Choroid plexus epithelial cells form the BCSFB, which is more permissive than the BBB (28). The BBB and BCSFB, as physical barriers, restrict the compounds that reach the CNS and prevent many valuable therapeutic molecules from reaching their targets in the CNS. However, several peptides and proteins can cross the BBB by transendothelial diffusion (29, 30, 31), and antibodies can cross the BBB after peripheral injection by mechanisms related to adsorptive endocytosis/transcytosis (32, 33).

In this study, we evaluated the serum half-life and BBB/BCSFB permeability of rh proSP-C and Bri2 BRICHOS after intravenous (i.v.) administration in WT mice. rh Bri2 BRICHOS forms different quaternary structures with distinct chaperone functions (18), and here we investigated rh Bri2 BRICHOS monomers, dimers, and oligomers individually. Both rh proSP-C and Bri2 BRICHOS were detected in the CSF, but only rh Bri2 BRICHOS domains reached the brain parenchyma after peripheral administration.

Results

Study design

The serum half-life and permeability through the BBB and BCSFB of rh proSP-C and Bri2 BRICHOS domains was studied by injecting them into the lateral tail vein of adult WT mice. Blood and CSF samples were collected and analyzed at different time points, as schematized in Fig. 1. The presence of injected rh BRICHOS domains in the brain parenchyma was evaluated by Western blots with or without prior immunoprecipitation, ELISA, and immunohistochemistry. The penetrance of rh BRICHOS domains into the CSF was assessed by Western blotting. The detection of rh proSP-C BRICHOS in the brain was

not expected to be affected by the presence of the endogenous protein because proSP-C is exclusively expressed in the lungs (21, 22).

To avoid the risk of interference with endogenous Bri2 present in brain tissue, an AU1 tag was added to rh Bri2 BRICHOS. The six-amino-acid-long AU1 tag was placed at the C-terminal end, and rh Bri2 BRICHOS-AU1 showed very similar chromatographic behavior and inhibitory effects against $A\beta 42$ fibril formation as WT rh Bri2 BRICHOS. In addition, Western blot analysis showed that there is no cross-reactivity between rh Bri2 BRICHOS and anti-AU1 antibodies (Fig. S1).
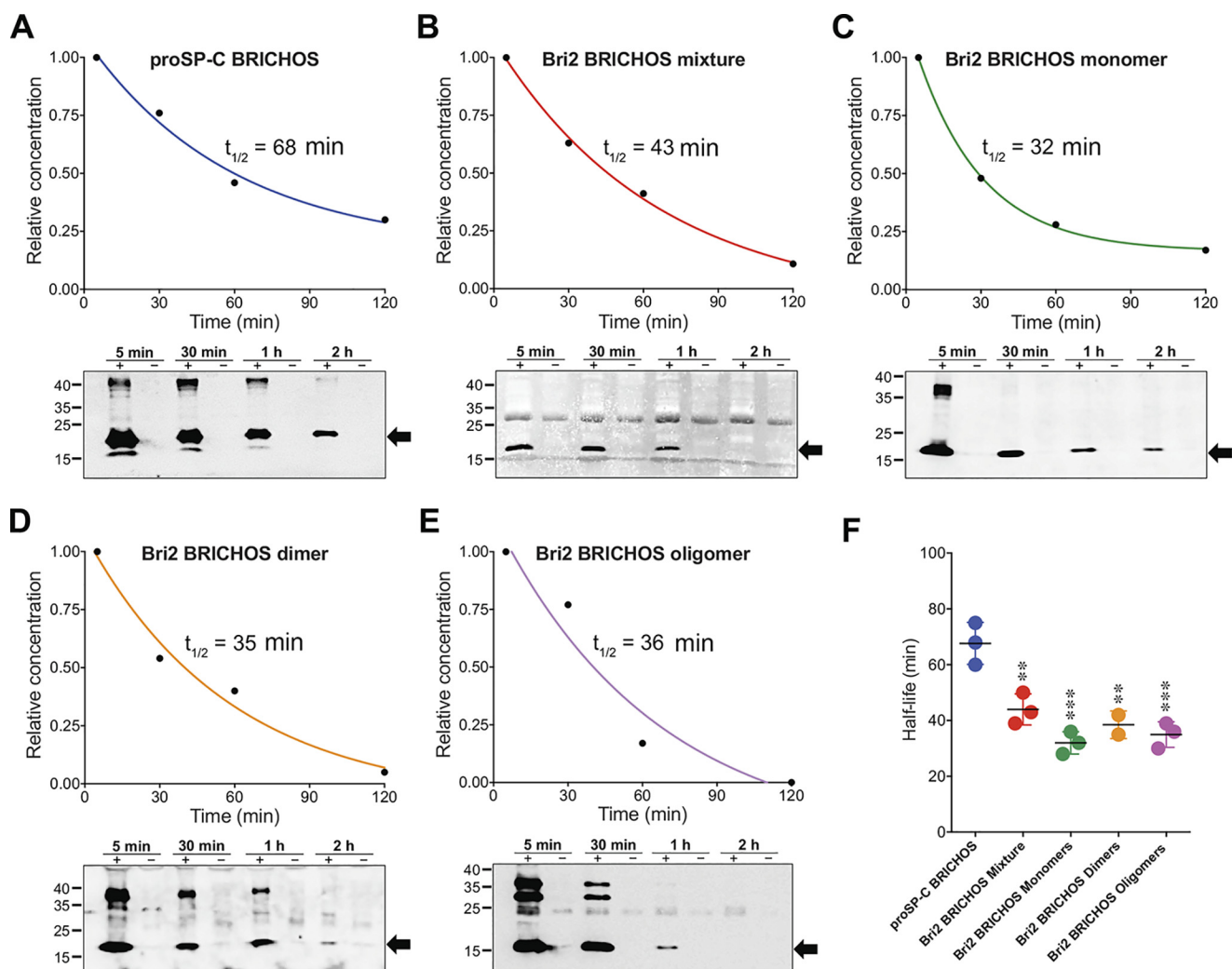
Serum half-lives of the rh Bri2 and proSP-C BRICHOS domains

The apparent serum half-lives of all tested rh BRICHOS domains were evaluated based on relative band intensities from Western blot analysis of blood samples withdrawn from the injected mice. The half-lives were calculated from the disappearance of the monomeric forms identified by reducing SDS-PAGE at 18 kDa for rh proSP-C and 17 kDa for rh Bri2 BRICHOS-AU1 (Fig. 2). rh proSP-C BRICHOS showed a half-life of 68 min in serum, which is significantly higher compared with 43 min for rh Bri2 BRICHOS-AU1 mixture and 32, 39, and 38 min for isolated rh Bri2 BRICHOS-AU1 monomers, dimers, and oligomers, respectively (Fig. 2, *A–F*). The differences in half-lives between the isolated rh Bri2 BRICHOS-AU1 forms were not statistically significant (Fig. 2*F*). Calculation of the half-lives from the disappearance of the monomer band but from SDS-PAGE run under nonreducing conditions showed shorter half-lives for all BRICHOS variants (Fig. S2). This suggests that disulfide-dependent oligomerization of BRICHOS monomers occurs in serum, as observed previously when rh Bri2 BRICHOS was incubated in mouse serum *ex vivo* (18).

Detection of rh proSP-C and Bri2 BRICHOS in the brain by Western blotting, immunoprecipitation, and ELISA

rh proSP-C BRICHOS was injected intravenously in doses from 10 to 50 mg/kg, and BBB permeability was evaluated after 2, 6, and 24 h (Fig. 1). In none of the treated mice could rh proSP-C BRICHOS be detected in the brain homogenate by Western blotting or in brain sections by immunohistochemistry (Fig. 3, *A and F*, and Figs. S3–S5). Rh Bri2 BRICHOS was injected in doses from 5 to 50 mg/kg, and brain samples were collected and analyzed 1, 2, 6, and 24 h after injection. Western

Figure 2. Serum half-lives of rh proSP-C and Bri2 BRICHOS after systemic injection. *A–E,* representative decay curves and Western blots of individual mice for rh proSP-C BRICHOS (*A*), the rh Bri2 BRICHOS-AU1 mixture (*B*), and isolated rh Bri2 BRICHOS-AU1 monomers (*C*), dimers (*D*), and oligomers (*E*). The half-lives were determined by densitometry of Western blot bands corresponding to the monomers (indicated by *arrows*). Bands corresponding to BRICHOS dimers and oligomers, which resist complete reduction, in particular for oligomers of rh Bri2 BRICHOS-AU1, were observed. A nonspecific band between 25–35 kDa of unknown origin was observed in *B*, *D*, and *E*. Western blot analysis was performed using an anti-S tag and anti-AU1 tag for the detection of rh proSP-C and Bri2 BRICHOS, respectively. The time points above the gels refer to minutes after injection, and lanes marked with + refer to samples from mice injected with 20 mg/kg rh BRICHOS; − denotes controls injected with PBS. *F,* summary of rh BRICHOS half-lives from two (rh Bri2 BRICHOS-AU1 dimers) or three (all other groups) different mice. The *error bars* show mean values and standard deviations. **, $p < 0.001$; ***, $p < 0.0001$ *versus* proSP-C BRICHOS.

blot analysis of the brain homogenates from mice treated with the rh Bri2 BRICHOS mixture revealed, in the majority of samples, a band corresponding to the molecular weight of the monomeric injected recombinant protein, whereas in control samples, the corresponding band was absent (Fig. 3*B*). Fig. 3*C* shows representative Western blot results obtained with brain samples collected 1, 2, and 6 h after injection of 20 mg/kg rh Bri2 BRICHOS-AU1 mixture. The band seen after 2 h (Fig. 3*C*) is detectable, although faint, after a short exposure time (Fig. S3*C*). A semiquantitative analysis of the rh Bri2 BRICHOS-AU1 band in samples collected 2 h after injection compared with an internal standard revealed a concentration of rh Bri2 BRICHOS-AU1 in the brain homogenate of about 20 ng/mg of total brain protein, which corresponds to 200 nM rh Bri2 BRICHOS-AU1. To increase the detection of the delivered rh Bri2 BRICHOS-AU1 in the brain homogenate, immunoprecipitation of the samples was performed prior to Western blot analysis using an antibody against the AU1 tag. Western blot of

the immunoprecipitated material showed a clear band corresponding to rh Bri2 BRICHOS-AU1 in brains collected 2 h after injection and a weaker band after 6 h (Fig. 3*D*). The entire gels of Fig. 3, *A–D,* shown in Fig. S3, reveal the presence of unspecific bands in samples from rh BRICHOS-injected mice and also in the PBS controls, but in all cases, they migrated slower than rh BRICHOS. In support of the immunoprecipitation data, analysis of the brain homogenates by ELISA revealed the presence of rh Bri2 BRICHOS-AU1 in the brains 2 h after injection (Fig. 3*E*). The average concentration of BRICHOS detected by ELISA was about 390 nM, corresponding to 0.4–0.5% of the total amount of rh Bri2 BRICHOS-AU1 injected intravenously. The range of rh Bri2 BRICHOS-AU1 amounts detected in brain tissue by ELISA span 0.1% to 1% of the total amount. 1 and 6 h after injection, about 70 and 90 nM, respectively, of rh Bri2 BRICHOS-AU1 were detected in brain homogenates (Fig. 3*E*). Considering all mice treated with rh Bri2 BRICHOS or Bri2 BRICHOS-AU1, the injected protein was detected in the brain
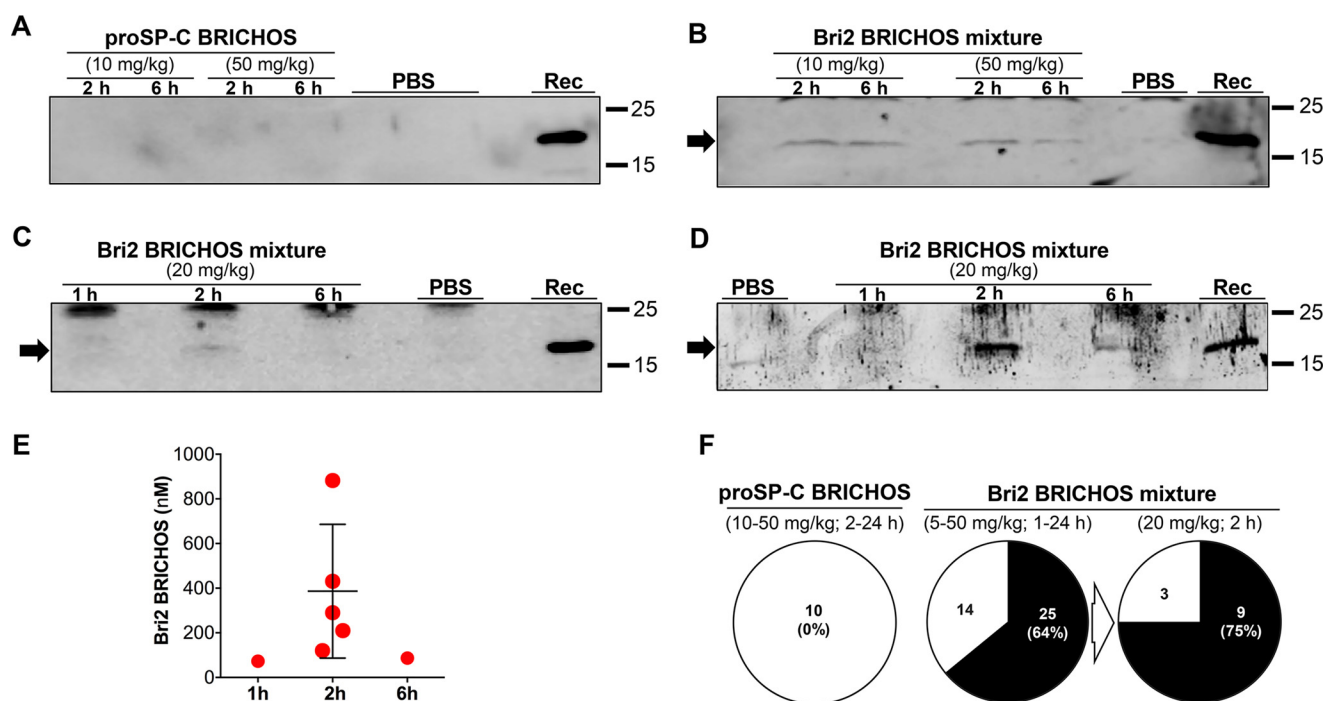
Figure 3. Rh Bri2, but not proSP-C BRICHOS, is detected in the mouse brain after intravenous injection. *A–D*, Western blot analysis of brain homogenates collected 1, 2, or 6 h after injection of rh proSP-C BRICHOS using an anti-S tag (*A*) or rh Bri2 BRICHOS using an anti-Bri2 BRICHOS antibody (*B*) and an anti-AU1 tag antibody (*C* and *D*) and PBS-injected controls. Rh Bri2 BRICHOS-AU1 (*D*) from the same sample as in *C* was immunoprecipitated. Lanes marked *Rec* indicate the migration of purified rh proSP-C or Bri2 BRICHOS-AU1. *E*, sandwich ELISA quantification of rh Bri2 BRICHOS-AU1 in brain homogenates 1, 2, and 6 h after injection of 20 mg/kg. Each point represents data from one mouse, and the *error bar* shows mean value and standard deviations. *F*, extent of detected rh proSP-C BRICHOS, rh Bri2 BRICHOS, or rh Bri2 BRICHOS-AU1 in the brain tissue of all injected mice. The dose ranges and times between injection and sampling used are given in *parentheses* above each *circle*. For the 5–50 mg/kg injections, both rh Bri2 BRICHOS and rh Bri2 BRICHOS-AU1 were used, whereas for the 20 mg/kg injections chart, only rh Bri2 BRICHOS-AU1 was used. In the *circles*, the *numbers* in each sector refer to the total number of mice in which rh BRICHOS was detected (*black sectors*) or not detected (*white sectors*) by Western blotting, immunoprecipitation, or ELISA in brain tissue. The percentages in *parentheses* refer to the extent of rh BRICHOS detection in brain tissue. The entire gels for *A–D* are shown in Fig. S3.

parenchyma in 64% of all cases (Fig. 3*F*). A higher detection rate (9 of 12 cases, 75%) was obtained in mice treated with 20 mg/kg of rh Bri2 BRICHOS-AU1 and analyzed 2 h after injections (Fig. 3*F*). Of the nine positive cases, rh Bri2 BRICHOS-AU1 was detected by ELISA in five mice, as reported in Fig. 3*E*, and by Western blotting in four mice. ELISA, Western blotting, and immunohistochemistry (see further below) were used for analysis of all three negative cases.

Last, to investigate the role of Bri2 BRICHOS oligomerization in BBB passage, isolated rh Bri2 BRICHOS-AU1 monomers, dimers, and oligomers were injected intravenously at a dose of 20 mg/kg, and the presence of rh Bri2 BRICHOS-AU1 was analyzed in brain tissue. Rh Bri2 BRICHOS-AU1 was detected by immunoprecipitation after injection of the monomer and dimer (Fig. 4, *A* and *B*). A band corresponding to a slightly slower-migrating species of unknown identity is seen in mice injected with rh Bri2 BRICHOS monomer and also in one of the two PBS controls (Fig. 4*A*). In contrast, no rh Bri2 BRICHOS-AU1 was detected in brain homogenates after injection of oligomers (Fig. 4*C*). For Bri2 BRICHOS-AU1 monomers, three mice gave positive detection on one occasion (Fig. 4*A*), but on another occasion, only a sample from one of these mice showed a positive signal (Fig. 4*B*). This shows that, in addition to the interindividual variability in observed passage over the BBB (Fig. 3*F*), there is also intraindividual variability in the extent of detection.
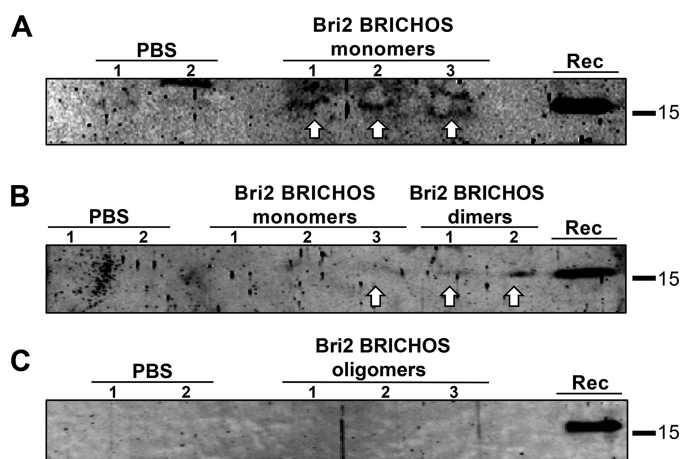

Figure 4. Rh Bri2 BRICHOS-AU1 is detected in the mouse brain after intravenous injection of monomers and dimers but not oligomers. *A–C*, immunoprecipitation using rabbit polyclonal anti-AU1 antibody coupled with protein A–Sepharose beads followed by Western blotting analysis with a goat polyclonal anti-Bri2 BRICHOS antibody of brain homogenates collected 2 h after injection of rh Bri2 BRICHOS-AU1 monomers or dimers (*A* and *B*), oligomers (*C*), or PBS-injected controls. *A* and *B* include results obtained for the same three mice injected with monomeric Bri2 BRICHOS-AU1. Lanes marked *Rec* show migration of rh Bri2 BRICHOS-AU1.

Detection of rh proSP-C and Bri2 BRICHOS in CSF by Western blotting

The permeability through the BCSFB of both the rh Bri2 BRICHOS-AU1 and rh proSP-C domains was evaluated by Western blot analysis of CSF. Three mice were treated with 20
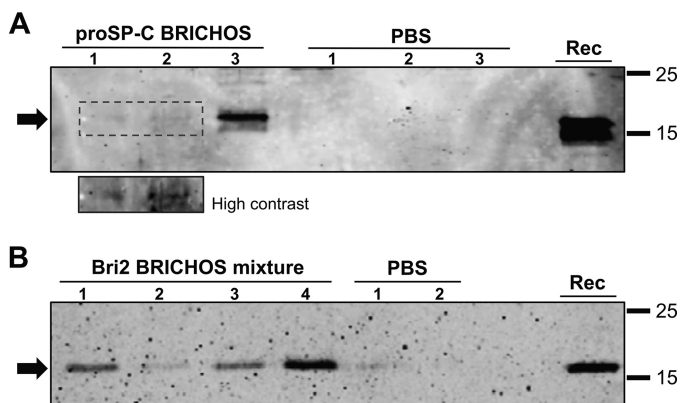
Figure 5. Rh proSP-C and Bri2 BRICHOS-AU1 are found in CSF after systemic injection. *A* and *B*, Western blots of CSF collected 2 h after intravenous injection of rh proSP-C BRICHOS in three mice using an anti-S tag antibody (*A*) and rh Bri2 BRICHOS-AU1 mixture in four mice using an anti-AU1 tag antibody (*B*) and PBS-injected controls. The *small panel* in *A* provides a higher-contrast version of the area outlined as a *dotted box*. Lanes marked *Rec* show the migration of purified rh proSP-C or Bri2 BRICHOS-AU1.

mg/kg rh proSP-C BRICHOS, and four mice were treated with the same dose of rh Bri2 BRICHOS-AU1. As shown in Fig. 5, proSP-C and Bri2 BRICHOS-AU1 were both detected in the CSF of all samples analyzed, although the proSP-C BRICHOS bands were on the border of detection in two cases (Fig. 5*A*). Potential blood contamination of CSF as a cause of BRICHOS detection was evaluated by examining the presence of hemoglobin, which should not be present in CSF (34). The results showed lack of hemoglobin immunoreactivity in CSF samples (Fig. S6*A*), which supports that rh BRICHOS domains permeate the BCSFB. rh Bri2 BRICHOS-AU1 was also detected in brain homogenates by immunoprecipitation and Western blot analysis of all four mice used for the CSF collection (Fig. S6*B*).

Immunohistochemical identification of rh proSP-C and Bri2 BRICHOS in the brain

Mouse brain slices from the prefrontal cortex, hippocampal area, striatum, and cerebellum were analyzed by immunohistochemistry to further evaluate and localize rh proSP-C and rh Bri2 BRICHOS after i.v. injection. Rh Bri2 BRICHOS-AU1 immunoreactivity was observed in the choroid plexus and, in most samples, in the cortex 2 h after i.v. injection (Fig. 6, *A–L*). In some cases, immunoreactivity was also observed in the striatum (Fig. 6, *M–O*, and Fig. S6) and in the hippocampal sulcus (Fig. 6*P*), whereas rh Bri2 BRICHOS immunoreactivity was never detected in the hippocampus or cerebellum. Some of the staining observed in the cortex and striatum was localized intracellularly in the perinuclear area (Fig. 6, *K and L*, and Fig. S7). Immunohistochemical staining for rh Bri2 BRICHOS-AU1 of mice injected with rh proSP-C BRICHOS was negative (Fig. S5), showing that Bri2 BRICHOS-AU1 immunoreactivity is not an artifactual result of injection of a recombinant protein purified from bacteria. In agreement with the immunoprecipitation and Western blot results, rh proSP-C BRICHOS could not be detected in any brain region, including the choroid plexus, after i.v. injection (Fig. S5).

Interestingly, positive staining for rh Bri2 BRICHOS-AU1 was identified in the choroid plexus of mice treated with the isolated dimeric species and also in one of the mice treated with
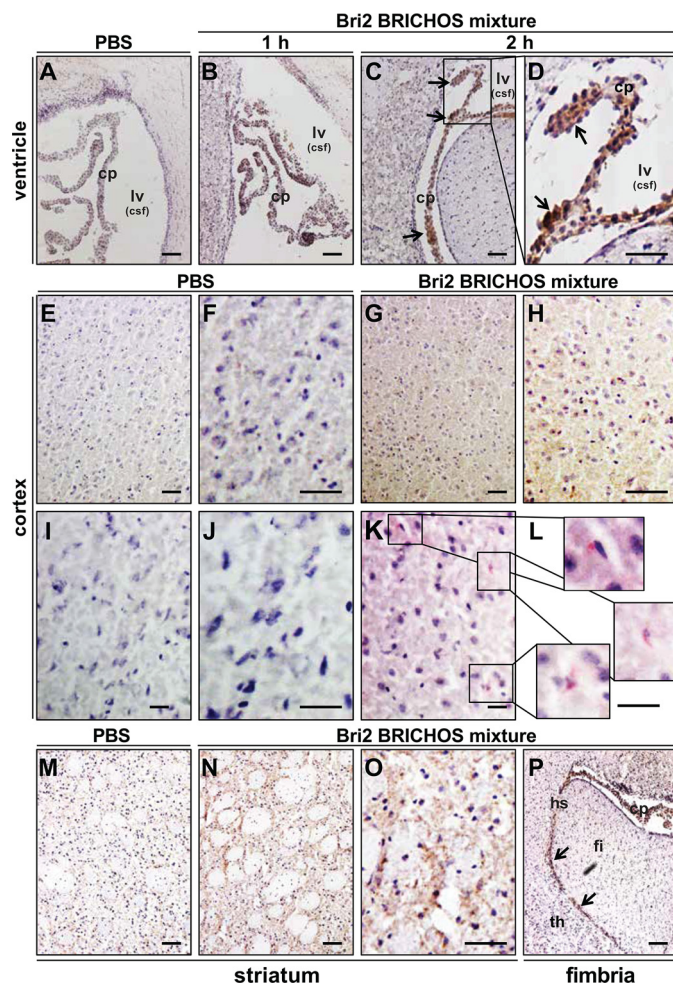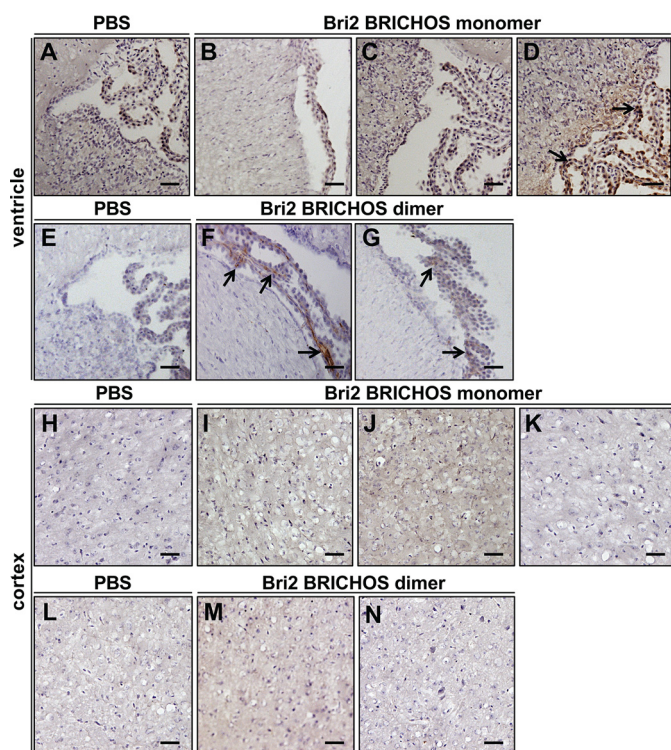

Figure 6. Rh Bri2 BRICHOS-AU1 is found in the plexus choroideus, cortex, and striatum after systemic injection. *A–P*, the lateral ventricle and surrounding tissue (*A–D*), cortical coronal sections (*E–L*), the striatum area (*M–O*), and fimbria/thalamic area (*P*) collected 1 or 2 h after injection of rh Bri2 BRICHOS-AU1 mixture (20 mg/kg) (*B–D*, *G*, *H*, *K*, *L*, and *N–P*) or PBS (*A*, *E*, *F*, *I*, *J*, and *M*). Tissues in *A–H* and *M–P* were stained with a mouse anti-AU1 antibody, followed by a secondary HRP-conjugated antibody and development with DAB staining. Tissues in *I–L* were stained with a rabbit anti-AU1 antibody followed by an AP-conjugated secondary antibody and development with permanent AP red solution. All samples were counterstained with hematoxylin. The *arrows* and *boxes* highlight areas with positive staining. *cp*, choroid plexus; *lv*, lateral ventricle; *csf*, cerebrospinal fluid; *fi*, fimbria; *hs*, hippocampal sulcus; *th*, thalamus. *Scale bars* = 50 μm in *A–H* and *M–P* and 25 μm in *I–L*.

the isolated monomers (Fig. 7, *A–G*). Staining was also found in the cortex of mice treated with monomeric and dimeric Bri2 BRICHOS-AU1 (Fig. 7, *H–N*). No rh Bri2 BRICHOS-AU1 was observed after injection of oligomeric species (data not shown).

Discussion

The long row of failed AD clinical trials emphasizes the importance to develop new strategies that are able to counteract the onset and course of this disease (35). Protein therapeutic agents, and in particular chaperones, could potentially be used to treat AD and other neurodegenerative disorders that are characterized by the accumulation of aggregated protein (36). Unfortunately, many potential protein-based drugs cannot be used in therapy, as they have low or no capacity to reach the brain parenchyma after parenteral administration (37, 38).

Figure 7. Rh Bri2 BRICHOS-AU1 is found in the plexus choroideus and cortex after systemic injections of monomers or dimers. *A–N*, lateral ventricle and surrounding tissue (*A–G*) and cortical coronal sections (*H–N*) collected 2 h after injection of 20 mg/kg rh Bri2 BRICHOS-AU1 monomer, dimer, or PBS and stained with mouse anti-AU1 antibody followed by a secondary HRP-conjugated antibody and development with DAB solution. The sections show the results obtained from three mice treated with rh Bri2 BRICHOS-AU1 monomers and two mice treated with rh Bri2 BRICHOS-AU1 dimers. The *arrows* highlight areas with positive staining in the choroid plexus. All samples were counterstained with hematoxylin. *Scale bars* = 50 µm.

In this study, we examined the ability of two recombinant chaperone-like domains, proSP-C and Bri2 BRICHOS, to cross the BBB and BCSFB. When delivered by i.v. injection into WT mice, the rh Bri2 BRICHOS mixture was found in the CSF in 100% of the injected mice and in the brain parenchyma in about 70% of the cases. Even though rh proSP-C BRICHOS showed a longer serum half-life compared with rh Bri2 BRICHOS, it was only found in the CSF and not in the brain parenchyma.

The BRICHOS domains of proSP-C and Bri2 are potent inhibitors of Aβ40 and Aβ42 fibrillation and neurotoxicity *in vitro* and *ex vivo* (9, 12–18, 39). Transgenic co-expression of either the proSP-C or Bri2 BRICHOS domain together with Aβ42 in the *Drosophila* CNS or eyes gives rise to an increase in soluble Aβ42, less aggregated Aβ, and attenuation of the AD-like phenotype, including improved locomotor function and increased longevity (19, 20). A delay in amyloid plaque formation and complete absence of cognitive decline were observed when a Bri2-Aβ42 fusion protein was used to express Aβ42 in the mouse brain (40), suggesting that co-expression of Bri2 BRICHOS alleviates Aβ42 neurotoxicity (19). The rh Bri2 BRICHOS concentrations detected in brains after intravenous injection (120–880 nM) were higher than the soluble Aβ40 and Aβ42 concentrations reported in different regions of AD post-mortem brain tissues (30–120 pM) (41). Aβ42 aggregation is extensively delayed (9), and most importantly, Aβ42 toxicity to

hippocampal slice preparations is reduced in the presence of substoichiometric concentrations of rh Bri2 BRICHOS (18); we speculate that the amounts of rh Bri2 BRICHOS that reach the brain after parenteral administration could effectively inhibit Aβ fibril formation and toxicity. Rh proSP-C BRICHOS was not detected in brain tissue after i.v. injection, but it was found in the CSF. The rh proSP-C BRICHOS domain forms a homotrimer (15, 42, 43), a phenomenon that may influence the ability to pass through the BBB. Likewise, larger oligomeric assemblies of rh Bri2 BRICHOS (18), consisting of 20–30 subunits, were apparently less prone to cross the BBB compared with the monomer and dimer, further suggesting that the assembly states affect the ability of BRICHOS to cross the BBB. Rh Bri2 BRICHOS was not found in all brain samples analyzed, which could be because the ratio of oligomers to monomers and dimers is increased at higher total BRICHOS concentration (Fig. S8), and the equilibrium could probably be altered after injection because the monomeric Bri2 BRICHOS reformed large oligomers in mouse serum (18). This might also explain why higher doses of rh Bri2 BRICHOS (50 mg/kg) and longer times between injection and analysis (24 h) did not result in increased amounts of Bri2 BRICHOS in the brain. Notably, rh Bri2 BRICHOS monomers potently prevent neuronal toxicity of Aβ42, whereas dimers most efficiently suppress Aβ42 fibril formation; high-molecular-weight oligomers are less efficient in reducing Aβ42 aggregation and toxicity but are very efficient inhibitors of nonfibrillar protein aggregation (18). Our results suggest that the different assembly states of rh Bri2 BRICHOS behave in different ways after *in vivo* administration because monomers (17 kDa) and dimers (34 kDa) apparently pass the BBB more efficiently than the larger oligomers (340–510 kDa) despite similar serum half-lives for all species. Further studies are needed to clarify the underlying mechanism by which rh Bri2 BRICHOS crosses the BBB.

A common view is that only molecules less than 400–500 Da in size can cross the BBB (44), but several examples of proteins that are able to cross the BBB have been described, including erythropoietin (34 kDa) (45), the exogenous tracer horseradish peroxidase (44 kDa) (30, 31), and serum proteins (29). Moreover, anti-Aβ antibodies (about 150 kDa) are able to enter the brain, bind to amyloid plaques, and cause a reduction in plaque burden in AD mouse models (32, 33) and in AD patients (46). BBB permeability is not the same throughout the brain, and local mechanisms may specifically regulate the transport of different molecules and proteins (47). It has been shown that specialized brain regions, such as the choroid plexus, circumventricular areas, and the subependymal zone, have higher permeability than the rest of the brain (31). These facts justify a brain region–specific distribution of exogenous protein-based compounds (30, 31). Interestingly, positive staining for rh Bri2 BRICHOS was observed in the choroid plexus region. The choroid plexus contains more permeable capillaries compared with the rest of the brain and is involved in many aspects of blood–CNS exchange, including drug penetrance (48). These properties of the BCSFB probably explain the presence of both rh proSP-C and Bri2 BRICHOS in the CSF after systemic injection. A previous study has shown that CSF from AD patients has lower levels of the extracellular chaperones clusterin, hap-

toglobin, and α_2-macroblobulin compared with healthy control samples. AD CSF samples were toxic to neuroblastoma cells in culture, and re-establishing the physiological concentrations of extracellular chaperones in AD CSF protected neuroblastoma cells from Aβ toxicity (49). In addition, AD is associated with morphological changes in choroid plexus epithelial cells and compromised production of CSF (50). Intracerebroventricular injection of Aβ42 oligomers in mice increased the levels of pro-inflammatory cytokines in the CSF. This also affected choroid plexus epithelial cell morphology and tight junction protein levels. These changes were associated with loss of BCSFB integrity, as shown by an increase in BCSFB leakage (50). Histological alteration of the choroid plexus was observed in post-mortem AD patients (51). The choroid plexus is considered to be a possible target for AD treatment. The anti-Aβ42 toxicity properties of BRICHOS and the presence of rh proSP-C and Bri2 BRICHOS in the CSF after systemic administration lead us to believe that recombinant BRICHOS domains, in particular rh Bri2 BRICHOS, may have a beneficial impact on preventing CSF toxicity and BCSFB dysfunction.

The BBB and the BCSFB are both rich in transport mechanisms by which solute molecules move across membranes; only small lipophilic molecules can be transported passively across the cell. Some plasma proteins and other constituents can be actively transported across endothelial cell membranes by carrier- or receptor-mediated transporters and transcytosis, but it is thought that the majority of BBB transporters have yet to be discovered (52). Bri2 is expressed in peripheral tissues and in the brain, in particular in the hippocampus, cortex, and cerebellum (23, 24). The expression of Bri2 in both peripheral tissues and CNS may suggest the existence of a system for cross-talk between these sites. ProSP-C, in contrast, is expressed exclusively in the alveolar epithelium, and rh proSP-C BRICHOS could not be detected in the brain after systemic administration. The presence of rh Bri2 BRICHOS in the choroid plexus and CSF will contribute to the protein detected by Western blots and ELISA of brain homogenates. However, our immunohistochemical results indicate that injected Bri2 BRICHOS is also localized in other brain regions and intracellularly.

In conclusion, the results presented here provide a new incentive to explore the BRICHOS domains, and in particular rh Bri2 BRICHOS, as a potential therapeutic tool for the treatment of neurodegenerative disorders. Systemic administration of rh Bri2 BRICHOS in mouse models of AD will be necessary to evaluate the potential of BRICHOS therapy.

Experimental procedures

Recombinant proteins

Rh proSP-C BRICHOS—Cloning, expression, and purification were performed as described previously (15, 43). Briefly, the cells were lysed for 30 min with 1 mg/ml lysozyme and incubated with DNase and 2 mM MgCl$_2$ for 30 min on ice. The cell lysate was centrifuged at 6000 $\times$ g for 20 min, and the pellet was suspended in 20 mM Tris (pH 8.0) containing 2 M urea and 0.1 M NaCl and sonicated for 5 min. After 30 min of centrifugation at 30,000 $\times$ g at 4 °C, the supernatant was collected, filtered

through a 4.5-μm filter, and poured on a nickel–agarose column (Qiagen, Ltd., West Sussex, UK). The column was washed with 50 ml of 20 mM Tris (pH 8.0) containing 0.1 M NaCl and urea with progressively decreased concentration; *i.e.* 2, 1, and 0 M. The target protein was finally eluted with 200 mM imidazole in 20 mM Tris (pH 8.0) containing 0.1 M NaCl, dialyzed against 20 mM Tris (pH 8.0) with 0.05 M NaCl, cleaved by thrombin for 16 h at 4 °C (enzyme/substrate weight ratio of 0.002), and then reapplied to a nickel–agarose column to remove the released His$_6$ tag. The cleaved-off protein was further purified using ion exchange chromatography as described previously (53).

Rh Bri2 BRICHOS—The expression and purification of the rh Bri2 BRICHOS domain, corresponding to residues 113–231 of full-length human Bri2, have been described previously (18, 20). To enable specific immunodetection of injected rh Bri2 BRICHOS, a six-residue AU1 tag (DTYRYI) was added C-terminally by PCR amplification. The AU1-tagged rh Bri2 BRICHOS was expressed in *Escherichia coli* Shuffle T7 cells as a fusion protein with an N-terminal tag of His$_6$-NT*. The cells were grown at 30 °C in lysogeny broth medium containing 15 μg/ml kanamycin until A_{60} reached 0.7–0.9, and then the temperature was cooled down to 20 °C, and 0.5 mM isopropyl 1-thio-β-D-galactopyranoside was added. After overnight induction, the cells were harvested by centrifuge at 7000 $\times$ g for 20 min at 4 °C and resuspended in 20 mM Tris (pH 8.0). The cell suspension was sonicated on ice for 10 min (2 s on, 2 s off, 65% of the maximum amplitude) and centrifuged at 24,000 $\times$ g at 4 °C. The supernatant was collected and poured onto a nickel–agarose column equilibrated with 20 mM Tris-HCl (pH 8.0). The column was washed with 20 mM Tris-HCl (pH 8.0), followed by 20 mM Tris-HCl (pH 8.0) with 20 mM imidazole. The fusion protein was eluted with 300 mM imidazole in 20 mM Tris-HCl (pH 8.0) and dialyzed against 20 mM Tris-HCl (pH 8.0) containing thrombin (enzyme/substrate ratio of 0.001, Merck) for 16 h at 4 °C. The cleaved protein was reapplied onto the nickel–agarose column, and the cleaved-off rh Bri2 BRICHOS protein was collected. After concentration in a 5-kDa Vivaspin 20 column (GE Healthcare) at 4000 $\times$ g, samples were applied onto a PD-10 desalting column (GE Healthcare) and eluted with filtered and autoclaved 1$\times$ PBS (pH 7.4). Endotoxins were removed using a 0.50-ml Pierce high-capacity endotoxin removal column (Thermo Scientific). The final cleaved-off proteins were filtered through a 0.2-μm filter and stored at −20 °C. Different rh Bri2 BRICHOS species were separated and analyzed by Superdex 200 PG, 200 GL, or 75 PG columns (GE Healthcare) using an Äkta prime system (18).

Animal procedures

8- to 10-week-old C57BL/6NTac (Taconic) male mice were used. All mice were kept under controlled conditions of humidity and temperature on a 12-h light-dark cycle. Animals were group-housed (seven per cage) with food and water available *ad libitum*. The animal procedures were approved by the ethical committees of Södra Stockholm's Djurförsöksetiska Nämnd (dnr S 6 –15) and Linköping's etiska nämnd (ID855). The experimental scheme is shown in Fig. 1. Mice received a single i.v. injection into the lateral tail vein by using a 0.3-ml syringe with a 30-gauge needle. Rh proSP-C or Bri2 BRICHOS in PBS was

injected in a dose range of 5–50 mg/kg, and control mice received PBS only. The Rh proSP-C or Bri2 BRICHOS fractions were kept frozen and not brought to room temperature until about 30 min before the injection, and this procedure has been shown not to cause significant formation of larger species (18). Before the injection, mice were placed in a single cage and put under a heat lamp for 5 min to dilate the tail veins. The mice were anesthetized with ketamine (100 mg/kg) and xylazine (20 mg/kg) and perfused intracardially with 40 ml of saline (0.9% NaCl) 1, 2, 6, and 24 h after injection. Brains were quickly removed and divided into left and right hemispheres. All tissues were snap-frozen in dry ice and stored at −80 °C until analysis.

Serum collection

Blood samples were collected from the tail vein at different time points after rh BRICHOS proteins were injected (Fig. 1). The lateral tail vein was punctured using a 27-gauge needle, and 50–100 μl of blood was collected at each time point. Blood samples were centrifuged for 10 min at 3000 rpm (4 °C), and then the serum was collected and transferred into tubes and stored at −20 °C. Before analysis, the samples were diluted 1:5 in PBS.

CSF collection

CSF sampling was adapted from the method described by DeMattos (54). The mice were anesthetized and placed in the prone position in a stereotactic instrument. A sagittal incision of the skin was made inferior to the occiput. Under the dissection microscope, subcutaneous tissue and neck muscles through the midline were separated. The dura mater was exposed, and the area was washed with PBS to remove blood and tissue contamination. The dura mater was punched with a 27-gauge needle, and CSF was collected in a capillary tube. The volume of CSF obtained was ∼5–8 μl/mouse. All samples were stored in polypropylene tubes at −80 °C until analysis.

Antibodies

For Western blotting, primary antibodies and dilutions used were as follows: 1:3000 goat anti-proSP-C, 1:1000 rabbit anti-S tag, 1:250 goat anti-Bri2 BRICHOS, 1:1000 rabbit anti AU1, and 1:1000 rabbit anti hemoglobin (all from Abcam). Secondary antibodies conjugated with horseradish peroxidase (HRP) or anti-rabbit (GE Healthcare) or anti-goat (Life Technologies) Igs were diluted 1:5000. Fluorescently labeled secondary antibodies (Li-Cor), anti-rabbit or anti goat, were diluted 1:10,000. In the sandwich ELISA, goat anti-Bri2 BRICHOS was used as the capture antibody, diluted 1:250, whereas, as detection antibody, rabbit anti-AU1 diluted 1:2000 was used. Secondary HRP-conjugated antibodies were diluted 1:2000. In the immunohistochemistry experiments, the antibody dilutions were 1:500 and 1:1000 for goat anti-proSP-C, 1:500 for rabbit anti-proSP-C (ATLAS), 1:200 for rabbit anti-S tag, 1:500 for goat anti-Bri2 BRICHOS, 1:100 for mouse anti-AU1 (Biolegend), and 1:200 for rabbit anti-AU1. Secondary HRP-conjugated antibodies were diluted 1:200.

SDS-PAGE and Western blotting

Mouse tissues were homogenized in 50 mᴍ Tris-HCl (pH 7.4), 150 mᴍ NaCl, 1.0% (v/v) Triton X-100, 0.1% (w/v) SDS, and 10 mᴍ EDTA supplemented with protease inhibitors as described previously (55). Brain samples were centrifuged for 30 min at 14,000 rpm (4 °C), and then the supernatant was collected and stored at −20 °C. The protein concentrations were determined by the Bradford method. Serum, brain, and CSF samples were prepared in denaturing buffer containing 2% SDS, 0.03 ᴍ Tris, 5% 2-mercaptoethanol, 10% glycerol, bromphenol blue, and 2-mercaptoethanol (reducing conditions) or without 2-mercaptoethanol (nonreducing conditions) and heated for 10 min at 96 °C. The gel loading for serum and brain homogenates was normalized so that 100 μg of total proteins were loaded per well, whereas for CSF, the total sample amount obtained was loaded. The samples were separated on 10% or 13.5% SDS-PAGE gels and blotted on nitrocellulose membranes (GE Healthcare). After blotting, the membranes were blocked in 5% milk/PBS for 1 h, followed by incubation with primary antibody in 5% milk, 0.1% Tween/PBS for 1 h at room temperature or overnight at 4 °C. The membranes were washed three times with 0.1% Tween/PBS, and secondary antibodies in 5% milk and 0.1% Tween/PBS were added for 1 h at room temperature. After washing, enhanced chemoluminescence detection reagent (GE Healthcare) was added according to the manufacturer's protocol, and images were acquired using a CCD camera (LAS-3000) or a fluorescence imaging system (Li-Cor, Odyssey CLx).

Immunoprecipitation

5 mg of mouse brain homogenate was adjusted to a total volume of 400 μl in PBS and incubated by rotation at 4 °C overnight in the presence of 1:100 rabbit anti-AU1 antibody. Protein A–Sepharose beads (100 μg/ml, GE Healthcare) were added to the samples, incubated by rotation for 1 h at 4 °C, centrifuged at 400 × g for 3 min, washed with PBS, and again centrifuged twice. The pelleted material was boiled for 10 min in SDS loading buffer with β-mercaptoethanol and PBS, the supernatant was loaded on a 13.5% SDS-PAGE gel, and Western blotting was performed as described.

ELISA

For the sandwich ELISA, the capture antibody (goat anti-Bri2 BRICHOS) was loaded in 96-well (Nunc® MicroWell™) plates and incubated overnight at 4 °C. The plates were washed three times in 0.05% Tween/PBS and blocked with 1% BSA/PBS for 2 h. The samples (250 μg/ml) were incubated at room temperature for 2 h, followed by a primary antibody (rabbit anti-AU1) in 1% BSA and 0.05% Tween/PBS for 2 h at room temperature. The plate was washed, and a secondary anti-rabbit in 1% BSA and 0.05% Tween/PBS was added for 2 h at room temperature. After the washing step, 3,3′,5,5′-tetramethylbenzidine solution (100 μl/well) was added and incubated for 30 min at room temperature in the dark. The reaction was stopped by adding 100 μl/well of 0.5 ᴍ H_2SO_4. The absorbance was measured at 450 nm, using the values for ELISA of brain homogenates from PBS-injected control mice as blank. A standard curve was generated from analysis of rh proSP-C and Bri2 BRICHOS in a range from 0.1 to 64 ng. The amount of rh Bri2 BRICHOS-AU1 that reached the brain was estimated by assuming that the protein was evenly distributed in the whole

brain. For these calculations, a brain density of 1.04 g/ml (56), average brain weight of 486 mg, and average total protein in brain homogenates of 75 mg were used.

Immunohistochemistry

Coronal cryostat sections (10–20 μm) were thaw-mounted onto Superfrost Plus microscope slides. Brain sections were briefly washed in Tris-buffered saline prior to fixation in 4% formaldehyde solution for 5 min at room temperature. Sections were then incubated overnight at 4 °C with the primary antibodies. After washing with Tris-buffered saline, sections were incubated with HRP-conjugated secondary antibody for 45 min at room temperature and developed using a DAB (3,3′-diaminobenzidine) substrate kit (Vector Laboratories). In some experiments, slides were incubated with Mach 2 Double Stain2 containing conjugated secondary anti-rabbit alkaline phosphatase (AP) antibody (Biocare Medical). AP staining was visualized with permanent red (Biosite) solutions. Slides were counterstained in hematoxylin, dehydrated through graded alcohols, cleared in xylene, and then mounted with Permount.

Statistical analysis

Statistical analysis was performed using the GraphPad Prism program. Data were analyzed using one-way analysis of variance followed by Tukey's *post hoc* tests. Serums half-lives were calculated after densitometric analysis of the BRICHOS monomeric band intensities with ImageJ. The concentrations were expressed as relative intensities and normalized for each curve to the sample intensity at 5 min. The apparent half-life was obtained using GraphPad Prism by a nonlinear one-phase decay analysis.

References

1. Muchowski, P. J. (2002) Protein misfolding, amyloid formation, and neurodegeneration: a critical role for molecular chaperones? *Neuron* **35,** 9–12 CrossRef Medline
2. Serrano-Pozo, A., Frosch, M. P., Masliah, E., and Hyman, B. T. (2011) Neuropathological alterations in Alzheimer disease. *Cold. Spring Harb. Perspect. Med.* **1,** a006189 Medline
3. Mohandas, E., Rajmohan, V., and Raghunath, B. (2009) Neurobiology of Alzheimer's disease. *Indian J. Psychiatry* **51,** 55–61 CrossRef Medline
4. Karran, E., and De Strooper, B. (2016) The amyloid cascade hypothesis: are we poised for success or failure? *J. Neurochem.* **139,** 237–252 CrossRef Medline
5. Goure, W. F., Krafft, G. A., Jerecic, J., and Hefti, F. (2014) Targeting the proper amyloid-β neuronal toxins: a path forward for Alzheimer's disease immunotherapeutics. *Alzheimers Res. Ther.* **6,** 42 CrossRef Medline
6. Khan, A., Corbett, A., and Ballard, C. (2017) Emerging amyloid and tau targeting treatments for Alzheimer's disease. *Expert Rev. Neurother.* **17,** 697–711 CrossRef Medline
7. Sánchez-Pulido, L., Devos, D., and Valencia, A. (2002) BRICHOS: a conserved domain in proteins associated with dementia, respiratory distress and cancer. *Trends Biochem. Sci.* **27,** 329–332 CrossRef Medline
8. Hedlund, J., Johansson, J., and Persson, B. (2009) BRICHOS: a superfamily of multidomain proteins with diverse functions. *BMC Res. Notes* **2,** 180 CrossRef Medline
9. Willander, H., Presto, J., Askarieh, G., Biverstål, H., Frohm, B., Knight, S. D., Johansson, J., and Linse, S. (2012) BRICHOS domains efficiently delay fibrillation of amyloid β-peptide. *J. Biol. Chem.* **287,** 31608–31617 CrossRef Medline
10. Knight, S. D., Presto, J., Linse, S., and Johansson, J. (2013) The BRICHOS domain, amyloid fibril formation, and their relationship. *Biochemistry* **52,** 7523–7531 CrossRef Medline
11. Kallberg, Y., Gustafsson, M., Persson, B., Thyberg, J., and Johansson, J. (2001) Prediction of amyloid fibril-forming proteins. *J. Biol. Chem.* 276, 12945–12950 CrossRef Medline
12. Johansson, H., Nerelius, C., Nordling, K., and Johansson, J. (2009) Preventing amyloid formation by catching unfolded transmembrane segments. *J. Mol. Biol.* **389,** 227–229 CrossRef Medline
13. Nerelius, C., Gustafsson, M., Nordling, K., Larsson, A., and Johansson, J. (2009) Anti-amyloid activity of the C-terminal domain of proSP-C against amyloid β-peptide and medin. *Biochemistry* **48,** 3778–3786 CrossRef Medline
14. Peng, S., Fitzen, M., Jörnvall, H., and Johansson, J. (2010) The extracellular domain of Bri2 (ITM2B) binds the ABri peptide (1–23) and amyloid β-peptide (Aβ1–40): implications for Bri2 effects on processing of amyloid precursor protein and Aβ aggregation. *Biochem. Biophys. Res. Commun.* **393,** 356–361 CrossRef Medline
15. Willander, H., Askarieh, G., Landreh, M., Westermark, P., Nordling, K., Keränen, H., Hermansson, E., Hamvas, A., Nogee, L. M., Bergman, T., Saenz, A., Casals, C., Åqvistg, J., Jörnvall, J., Berglund, H., *et al.* (2012) High-resolution structure of a BRICHOS domain and its implications for anti-amyloid chaperone activity on lung surfactant protein C. *Proc. Natl. Acad. Sci. U.S.A.* **109,** 2325–2329 CrossRef Medline
16. Cohen, S. I. A., Arosio, P., Presto, J., Kurudenkandy, F. R., Biverstal, H., Dolfe, L., Dunning, C., Yang, X., Frohm, B., Vendruscolo, M., Johansson, J., Dobson, C. M., Fisahn, A., Knowles, T. P. J., and Linse, S. (2015) A molecular chaperone breaks the catalytic cycle that generates toxic Aβ oligomers. *Nat. Struct. Mol. Biol.* **22,** 207–213 CrossRef Medline
17. Arosio, P., Michaels, T. C., Linse, S., Månsson, C., Emanuelsson, C., Presto, J., Johansson, J., Vendruscolo, M., Dobson, C. M., and Knowles, T. P. (2016) Kinetic analysis reveals the diversity of microscopic mechanisms through which molecular chaperones suppress amyloid formation. *Nat. Commun.* **7,** 10948 CrossRef Medline
18. Chen, G., Abelein, A., Nilsson, H. E., Leppert, A., Andrade-Talavera, Y., Tambaro, S., Hemmingsson, L., Roshan, F., Landreh, M., Biverstål, H., Koeck, P. J. B., Presto, J., Hebert, H., Fisahn, A., and Johansson, J. (2017) Bri2 BRICHOS client specificity and chaperone activity are governed by assembly state. *Nat. Commun.* **8,** 2081 CrossRef Medline
19. Hermansson, E., Schultz, S., Crowther, D., Linse, S., Winblad, B., Westermark, G., Johansson, J., and Presto, J. (2014) The chaperone domain BRICHOS prevents CNS toxicity of amyloid-β peptide in *Drosophila melanogaster. Dis. Model. Mech.* **7,** 659–665 CrossRef Medline
20. Poska, H., Haslbeck, M., Kurudenkandy, F. R., Hermansson, E., Chen, G., Kostallas, G., Abelein, A., Biverstål, H., Crux, S., Fisahn, A., Presto, J., and Johansson, J. (2016) Dementia related Bri2 BRICHOS is a versatile molecular chaperone that efficiently inhibits Aβ42 toxicity in *Drosophila. Biochem. J.* **473,** 3683–3704 CrossRef Medline
21. Glasser, S. W., Korfhagen, T. R., Bruno, M. D., Dey, C., and Whitsett, J. A. (1990) Structure and expression of the pulmonary surfactant protein SP-C gene in the mouse. *J. Biol. Chem.* 265, 21986–21991 Medline
22. Glasser, S. W., Korfhagen, T. R., Wert, S. E., Bruno, M. D., McWilliams, K. M., Vorbroker, D. K., and Whitsett, J. A. (1991) Genetic element from human surfactant protein SP-C gene confers bronchiolar-alveolar cell specificity in transgenic mice. *Am. J. Physiol.* **261,** L349-L356 Medline
23. Lashley, T., Revesz, T., Plant, G., Bandopadhyay, R., Lees, A. J., Frangione, B., Wood, N. W., de Silva, R., Ghiso, J., Rostagno, A., and Holton, J. L. (2008) Expression of BRI2 mRNA and protein in normal human brain and familial British dementia: its relevance to the pathogenesis of disease. *Neuropathol. Appl. Neurobiol.* **34,** 492–505 CrossRef Medline

24. Baron, B. W., and Pytel, P. (2017) Expression pattern of the BCL6 and ITM2B proteins in normal human brains and in Alzheimer disease. *Appl. Immunohistochem. Mol. Morphol.* **25,** 489–496 CrossRef Medline

25. Del Campo, M., Hoozemans, J. J., Dekkers, L. L., Rozemuller, A. J., Korth, C., Müller-Schiffmann, A., Scheltens, P., Blankenstein, M. A., Jimenez, C. R., Veerhuis, R., and Teunissen, C. E. (2014) BRI2-BRICHOS is increased in human amyloid plaques in early stages of Alzheimer's disease. *Neurobiol. Aging* **35,** 1596–1604 CrossRef Medline

26. Dolfe, L., Tambaro, S., Tigro, H., Del Campo, M., Hoozemans, J. J. M., Wiehager, B., Graff, C., Winblad, B., Ankarcrona, M., Kaldmäe, M., Teunissen, C. E., Rönnbäck, A., Johansson, J., and Presto, J. (2018) The Bri2 and Bri3 BRICHOS domains interact differently with intracellular Aβ42 and Alzheimer amyloid plaques. *J. Alzheimers Dis. Rep.* **2,** 27–39 CrossRef Medline

27. Abbott, N. J., Patabendige, A. A., Dolman, D. E., Yusof, S. R., and Begley, D. J. (2010) Structure and function of the blood-brain barrier. *Neurobiol. Dis.* **37,** 13–25 CrossRef Medline

28. Johanson, C. E., Stopa, E. G., and McMillan, P. N. (2011) The blood-cerebrospinal fluid barrier: structure and functional significance. *Methods Mol. Biol.* **686,** 101–131 CrossRef Medline

29. Broadwell, R. D., and Sofroniew, M. V. (1993) Serum proteins bypass the blood-brain fluid barriers for extracellular entry to the central nervous system. *Exp. Neurol.* **120,** 245–263 CrossRef Medline

30. Ueno, M., Akiguchi, I., Hosokawa, M., Yagi, H., Takemura, M., Kimura, J., and Takeda, T. (1994) Accumulation of blood-borne horseradish peroxidase in medial portions of the mouse hippocampus. *Acta Neurol. Scand.* **90,** 400–404 Medline

31. Ueno, M., Akiguchi, I., Hosokawa, M., Kotani, H., Kanenishi, K., and Sakamoto, H. (2000) Blood-brain barrier permeability in the periventricular areas of the normal mouse brain. *Acta Neuropathol.* **99,** 385–392 CrossRef Medline

32. Bard, F., Cannon, C., Barbour, R., Burke, R. L., Games, D., Grajeda, H., Guido, T., Hu, K., Huang, J., Johnson-Wood, K., Khan, K., Kholodenko, D., Lee, M., Lieberburg, I., Motter, R., *et al.* (2000) Peripherally administered antibodies against amyloid β-peptide enter the central nervous system and reduce pathology in a mouse model of Alzheimer disease. *Nat. Med.* **6,** 916–919 CrossRef Medline

33. Banks, W. A., Terrell, B., Farr, S. A., Robinson, S. M., Nonaka, N., and Morley, J. E. (2002) Passage of amyloid β protein antibody across the blood-brain barrier in a mouse model of Alzheimer's disease. *Peptides* **23,** 2223–2226 CrossRef Medline

34. You, J. S., Gelfanova, V., Knierman, M. D., Witzmann, F. A., Wang, M., and Hale, J. E. (2005) The impact of blood contamination on the proteome of cerebrospinal fluid. *Proteomics* **5,** 290–296 CrossRef Medline

35. Cummings, J. L., Morstorf, T., and Zhong, K. (2014) Alzheimer's disease drug-development pipeline: few candidates, frequent failures. *Alzheimers Res. Ther.* **6,** 37 CrossRef Medline

36. Muchowski, P. J., and Wacker, J. L. (2005) Modulation of neurodegeneration by molecular chaperones. *Nat. Rev. Neurosci.* **6,** 11–22 CrossRef Medline

37. Brasnjevic, I., Steinbusch, H. W., Schmitz, C., Martinez-Martinez, P., and European NanoBioPharmaceutics Research Initiative (2009) European NanoBioPharmaceutics Research Initiative: delivery of peptide and protein drugs over the blood-brain barrier. *Prog. Neurobiol.* **87,** 212–251 CrossRef Medline

38. Pardridge, W. M. (2009) Alzheimer's disease drug development and the problem of the blood-brain barrier. *Alzheimers Dement.* **5,** 427–432 CrossRef Medline

39. Kurudenkandy, F. R., Zilberter, M., Biverstål, H., Presto, J., Honcharenko, D., Strömberg, R., Johansson, J., Winblad, B., and Fisahn, A. (2014) Amyloid-β-induced action potential desynchronization and degradation of hippocampal γ oscillations is prevented by interference with peptide conformation change and aggregation. *J. Neurosci.* **34,** 11416–11425 CrossRef Medline

40. Kim, J., Chakrabarty, P., Hanna, A., March, A., Dickson, D. W., Borchelt, D. R., Golde, T., and Janus, C. (2013) Normal cognition in transgenic BRI2-Aβ mice. *Mol. Neurodegener.* **8,** 15 CrossRef Medline

41. Collins-Praino, L. E., Francis, Y. I., Griffith, E. Y., Wiegman, A. F., Urbach, J., Lawton, A., Honig, L. S., Cortes, E., Vonsattel, J. P., Canoll, P. D., Goldman, J. E., and Brickman, A. M. (2014) Soluble amyloid β levels are elevated in the white matter of Alzheimer's patients, independent of cortical plaque severity. *Acta Neuropathol. Commun.* **2,** 83 CrossRef Medline

42. Casals, C., Johansson, H., Saenz, A., Gustafsson, M., Alfonso, C., Nordling, K., and Johansson, J. (2008) C-terminal, endoplasmic reticulum-lumenal domain of prosurfactant protein C: structural features and membrane interactions. *FEBS J.* **275,** 536–547 CrossRef Medline

43. Biverstål, H., Dolfe, L., Hermansson, E., Leppert, A., Reifenrath, M., Winblad, B., Presto, J., and Johansson, J. (2015) Dissociation of a BRICHOS trimer into monomers leads to increased inhibitory effect on Aβ42 fibril formation. *Biochim. Biophys. Acta* **1854,** 835–843 CrossRef Medline

44. Lipinski, C. A. (2000) Drug-like properties and the causes of poor solubility and poor permeability. *J. Pharmacol. Toxicol. Methods* **44,** 235–249 CrossRef Medline

45. Juul, S. E., McPherson, R. J., Farrell, F. X., Jolliffe, L., Ness, D. J., and Gleason, C. A. (2004) Erytropoietin concentrations in cerebrospinal fluid of nonhuman primates and fetal sheep following high-dose recombinant erythropoietin. *Biol. Neonate* **85,** 138–144 CrossRef Medline

46. Sevigny, J., Chiao, P., Bussière, T., Weinreb, P. H., Williams, L., Maier, M., Dunstan, R., Salloway, S., Chen, T., Ling, Y., O'Gorman, J., Qian, F., Arastu, M., Li, M., Chollate, S., *et al.* (2016) The antibody aducanumab reduces Aβ plaques in Alzheimer's disease. *Nature* **537,** 50–56 CrossRef Medline

47. Villaseñor, R., Kuennecke, B., Ozmen, L., Ammann, M., Kugler, C., Grüninger, F., Loetscher, H., Freskgård, P. O., and Collin, L. (2017) Region-specific permeability of the blood-brain barrier upon pericyte loss. *J. Cereb. Blood Flow Metab.* **37,** 3683–3694 CrossRef Medline

48. Liddelow, S. A. (2015) Development of the choroid plexus and blood-CSF barrier. *Front. Neurosci.* **9,** 32 Medline

49. Yerbury, J. J., and Wilson, M. R. (2010) Extracellular chaperones modulate the effects of Alzheimer's patient cerebrospinal fluid on Aβ(1–42) toxicity and uptake. *Cell Stress Chaperones* **15,** 115–121 CrossRef Medline

50. Brkic, M., Balusu, S., Van Wonterghem, E., Gorlé, N., Benilova, I., Kremer, A., Van Hove, I., Moons, L., De Strooper, B., Kanazir, S., Libert, C., and Vandenbroucke, R. E. (2015) Amyloid β oligomers disrupt blood-CSF barrier integrity by activating matrix metalloproteinases. *J. Neurosci.* **35,** 12766–12778 CrossRef Medline

51. Serot, J. M., Béné, M. C., Foliguet, B., and Faure, G. C. (2000) Morphological alterations of the choroid plexus in late-onset Alzheimer's disease. *Acta Neuropathol.* **99,** 105–108 CrossRef Medline

52. Sanchez-Covarrubias, L., Slosky, L. M., Thompson, B. J., Davis, T. P., and Ronaldson, P. T. (2014) Transporters at CNS barrier sites: obstacles or opportunities for drug delivery? *Curr. Pharm. Des.* **20,** 1422–1449 CrossRef Medline

53. Johansson, H., Nordling, K., Weaver, T. E., and Johansson, J. (2006) The Brichos domain-containing C-terminal part of pro-surfactant protein C binds to an unfolded poly-val transmembrane segment. *J. Biol. Chem.* **281,** 21032–21039 CrossRef Medline

54. DeMattos, R. B., Bales, K. R., Parsadanian, M., O'Dell, M. A., Foss, E. M., Paul, S. M., and Holtzman, D. M. (2002) Plaque-associated disruption of CSF and plasma amyloid-β (Aβ) equilibrium in a mouse model of Alzheimer's disease. *J. Neurochem.* **81,** 229–236 CrossRef Medline

55. Tambaro, S., Tomasi, M. L., and Bortolato, M. (2013) Long-term CB$_I$ receptor blockade enhances vulnerability to anxiogenic-like effects of cannabinoids. *Neuropharmacology* **70,** 268–277 CrossRef Medline

56. Barber, T. W., Brockway, J. A., and Higgins, L. S. (1970) The density of tissues in and about the head. *Acta Neurol. Scand.* **46,** 85–92 CrossRef Medline